

This discussion paper is/has been under review for the journal Atmospheric Chemistry and Physics (ACP). Please refer to the corresponding final paper in ACP if available.

Radiative impacts of cloud heterogeneity and overlap in an atmospheric GCM

L. Oreopoulos et al.

Radiative impacts of cloud heterogeneity and overlap in an atmospheric General Circulation Model

L. Oreopoulos¹, D. Lee^{1,2,3}, Y. C. Sud¹, and M. J. Suarez¹

¹NASA Goddard Space Flight Center, Greenbelt, MD, USA

²University Space Research Association, Columbia, MD, USA

³Seoul National University, Seoul, South Korea

Received: 16 April 2012 – Accepted: 24 April 2012 – Published: 12 May 2012

Correspondence to: L. Oreopoulos (lazaros.oreopoulos@nasa.gov)

Published by Copernicus Publications on behalf of the European Geosciences Union.

Title Page

Abstract

Introduction

Conclusions

References

Tables

Figures

⏪

⏩

◀

▶

Back

Close

Full Screen / Esc

Printer-friendly Version

Interactive Discussion

Abstract

The radiative impacts of introducing horizontal heterogeneity of layer cloud condensate, and vertical overlap of condensate and cloud fraction are examined with the aid of a new radiation package operating in the GEOS-5 Atmospheric General Circulation Model. The impacts are examined in terms of diagnostic top-of-the-atmosphere shortwave (SW) and longwave (LW) cloud radiative effect (CRE) calculations for a range of assumptions and parameter specifications about the overlap. The investigation is conducted for two distinct cloud schemes, the one that comes with the standard GEOS-5 distribution, and another which has been recently used experimentally for its enhanced cloud microphysical capabilities; both are coupled to a cloud generator allowing arbitrary cloud overlap specification. We find that cloud overlap radiative impacts are significantly stronger for the operational cloud scheme for which a change of cloud fraction overlap from maximum-random to generalized results to global changes of SW and LW CRE of $\sim 4\text{Wm}^{-2}$, and zonal changes of up to $\sim 10\text{Wm}^{-2}$. This is because of fewer occurrences compared to the other scheme of large layer cloud fractions and of multi-layer situations with large numbers of atmospheric layers being simultaneously cloudy, conditions that make overlap details more important. The impact on CRE of the details of condensate distribution overlap is much weaker. Once generalized overlap is adopted, both cloud schemes are only modestly sensitive to the exact values of the overlap parameters. We also find that if one of the CRE components is overestimated and the other underestimated, both cannot be driven towards observed values by adjustments to cloud condensate heterogeneity and overlap alone.

1 Introduction

With new computationally efficient approaches to treat cloud-radiation interactions now available, there are fewer reasons to retain the simplistic cloud descriptions that have persisted in General Circulation Models (GCMs) for many years. Clouds do no longer

ACPD

12, 12287–12329, 2012

Radiative impacts of cloud heterogeneity and overlap in an atmospheric GCM

L. Oreopoulos et al.

Title Page

Abstract

Introduction

Conclusions

References

Tables

Figures

⏪

⏩

◀

▶

Back

Close

Full Screen / Esc

Printer-friendly Version

Interactive Discussion



Radiative impacts of cloud heterogeneity and overlap in an atmospheric GCM

L. Oreopoulos et al.

Title Page

Abstract

Introduction

Conclusions

References

Tables

Figures

⏪

⏩

◀

▶

Back

Close

Full Screen / Esc

Printer-friendly Version

Interactive Discussion

have to be treated by the radiation schemes of these models as homogeneous slabs within large areas $O(10^4 \text{ km}^2)$, with fractional coverages and optical depths that have been greatly adjusted to compensate for known biases arising from their nonlinear interaction with radiation. While capturing the radiative effects of full-blown 3-D cloud heterogeneity may still be elusive, the representation of in-cloud horizontal heterogeneity of cloud condensate and two-point statistics of vertical correlations of condensate and cloud fraction within a one-dimensional radiative transfer framework is now feasible. As a matter of fact, the current work is one more study that amply demonstrates the viability of such an undertaking.

The main development that makes more complex cloud descriptions possible is the introduction of methods that perform radiative transfer in the cloudy portions of GCM grid cells in a stochastic manner (Pincus et al., 2003). The more complex cloud descriptions come from cloud generators producing horizontal and vertical cloud variability according to rules that are relatively easy to implement. The cloud fields from the generators can then be coupled with stochastically operating radiative transfer schemes that only “see” atmospheric subcolumns where cloud fraction is unity and condensate is horizontally invariable whenever a layer is cloudy. With the radiative transfer simplified, the sensitivity of the radiation budget to a variety of specifications that transform a gridcolumn’s cloud profile to a cloud field consisting of several subcolumns can be easily examined. What we should ultimately investigate is whether the effects of cloud complexity on the transfer of solar and thermal infrared radiation matter for the GCM’s climate. Such a study of the full impacts of interactions and feedbacks of the altered radiation fields with the multitude of the GCM’s dynamical and physical processes is left for the future. Here, we simply focus on diagnosing the possible range of radiative impacts of enhanced cloud complexity, an approach akin to that of Shonk and Hogan (2010).

In the following we will present the tools, assumptions, and experimental setup that allow us to examine the degree to which cloud complexity changes the cloud radiative impact (Sects. 2, 3, and 4). The availability of two cloud schemes in the GCM at hand

and our analysis approach provides the opportunity to investigate whether the same assumptions about cloud complexity imposed on different initial cloud fields can yield notably distinct radiative impacts (Sect. 5) and what causes the contrasting behaviour (Sect. 6).

2 Implementation of RRTMG into GEOS-5

The effects of cloud overlap (fraction and condensate) on the radiative fluxes can be captured best with radiation codes equipped with as much flexibility as possible in the representation of such overlap. This (along with improved representation of gaseous absorption) was one of the primary motivations for the implementation into the GEOS-5 Atmospheric General Circulation Model (AGCM, Rienecker et al., 2010; Molod et al., 2012) of the RRTMG radiation package (Clough et al., 2005), a faster version of the RRTM codes (Mlawer et al., 1997; Iacono et al., 2008) designed specifically for large scale models and consisting of a solar and thermal infrared component. Both components can be run in so-called Monte Carlo Independent Column Approximation (McICA) mode (Pincus et al., 2003). RRTMG with McICA has been implemented successfully into ECMWF's Integrated Forecasting System (Morcrette et al., 2008) and several other large scale models. Within the McICA framework, when the radiation code is employed on a number of atmospheric (sub)columns, full spectral integration over each column is replaced by stochastic (Monte Carlo) integration. A simplified mathematical expression of this process can be written as follows:

$$\bar{F} = \frac{1}{N} \sum_{n=1}^N F_n = \frac{1}{N} \sum_{n=1}^N \sum_{k=1}^K f_{n,k} \approx \sum_{k=1}^K f_{n_k,k} \quad (1)$$

The uppercase symbols of Eq. (1) represent broadband fluxes, while the lowercase letters represent pseudo-monochromatic fluxes per the correlated- k paradigm (Lacis and Oinas, 1991). \bar{F} represents a broadband flux (solar or thermal infrared; upward or

Radiative impacts of cloud heterogeneity and overlap in an atmospheric GCM

L. Oreopoulos et al.

Title Page

Abstract

Introduction

Conclusions

References

Tables

Figures

⏪

⏩

◀

▶

Back

Close

Full Screen / Esc

Printer-friendly Version

Interactive Discussion



Radiative impacts of cloud heterogeneity and overlap in an atmospheric GCM

L. Oreopoulos et al.

[Title Page](#)[Abstract](#)[Introduction](#)[Conclusions](#)[References](#)[Tables](#)[Figures](#)[⏪](#)[⏩](#)[◀](#)[▶](#)[Back](#)[Close](#)[Full Screen / Esc](#)[Printer-friendly Version](#)[Interactive Discussion](#)

downward) at any vertical level within the AGCM gridcolumn, F_n is a similar broadband flux for one of the N subcolumns generated by RRTMG's cloud generator (Räisänen et al., 2004, see below) within the gridcolumn, and $f_{n,k}$ is the pseudo-monochromatic flux for subcolumn n and spectral point k . What the above equation essentially conveys is that a broadband flux which is normally obtained by taking the average over N subcolumns of the sum of K spectral calculations for each subcolumn, is approximated by the sum of K spectral calculations where each spectral point k is paired randomly with one of the N subcolumns, n_k . Note that when using Eq. (1) the computational cost of the calculation over all subcolumns is the same as that of a full spectral integration of a single (sub)column. The performance of this approximation in large scale models has been tested extensively (e.g., Barker et al., 2008). The main issue of concern is whether the conditional random noise, decreasing as the inverse square root of the number of applications of Eq. (1), has any detrimental impact on the simulations. The prior studies and our test with GEOS-5 have shown that the McICA noise for sufficiently long runs (at least a month) is of similar length and nature as the internal variability of the model.

An extensive description of the brand of generator used in our implementation of RRTMG is provided by Räisänen et al. (2004). The cloud generator produces subcolumns that have either clear or completely overcast cloud layers. Whether the cloud condensate of a particular layer is different from one subcolumn to the next depends on the assumptions about horizontal cloud heterogeneity: either homogeneous or heterogeneous condensate distributions can be specified within the cloud generator. The horizontal location of clouds in a particular layer (i.e., subcolumn assignment) and specific value of condensate (for heterogeneous condensate distributions) depend on cloud presence at other layers according to the overlap rules implemented. By design, in the limit of an infinite number of subcolumns layer horizontal averages reproduce the vertical profile of cloud fraction and condensate provided as input to the generator by the AGCM. More specific descriptions of rules and assumptions about cloud fraction and

condensate distribution overlaps as implemented in the GEOS-5 cloud generator are provided in the section that follows.

3 Cloud overlap and variability representation

The cloud fraction overlap options for the cloud generator that comes with the RRTMG package include the standard assumptions that have been used extensively in the past, i.e., maximum, random, and (the most popular) maximum-random overlap (Geleyn and Hollingsworth, 1979; Tian and Curry, 1989) where contiguous cloudy layers overlap maximally and randomly otherwise. Räisänen et al. (2004) provides a mathematical description of the practical implementation of these overlap assumptions in a cloud generator algorithm. In this work, from the above simplified overlap descriptions, we only test the maximum-random overlap option.

Starting with the work of Hogan and Illingworth (2000), numerous studies (e.g., Mace and Benson-Troth, 2002; Oreopoulos and Khairoutdinov, 2003; Naud et al., 2008) have shown that the above simple overlap assumptions are inconsistent with cloud fields from observations and cloud resolving models, and that the concept of “generalized” cloud fraction overlap is more realistic. In the generalized overlap paradigm, the combined cloud fraction of two cloudy layers at heights z_1 and z_2 with separation distance $\Delta z = z_2 - z_1$ can be approximated as a weighted average of combined cloud fractions from maximum and random overlap, $C_{\max}(\Delta z)$ and $C_{\text{ran}}(\Delta z)$, respectively according to:

$$C(\Delta z) = \alpha(\Delta z)C_{\max}(\Delta z) + (1 - \alpha(\Delta z))C_{\text{ran}}(\Delta z) \quad (2)$$

with

$$C_{\max}(\Delta z) = \max(C(z_1), C(z_2)) \quad (3a)$$

$$C_{\text{ran}}(\Delta z) = 1 - (1 - C(z_1))(1 - C(z_2)) \quad (3b)$$

Radiative impacts of cloud heterogeneity and overlap in an atmospheric GCM

L. Oreopoulos et al.

Title Page

Abstract

Introduction

Conclusions

References

Tables

Figures

⏪

⏩

◀

▶

Back

Close

Full Screen / Esc

Printer-friendly Version

Interactive Discussion



Radiative impacts of cloud heterogeneity and overlap in an atmospheric GCM

L. Oreopoulos et al.

Title Page

Abstract

Introduction

Conclusions

References

Tables

Figures

⏪

⏩

◀

▶

Back

Close

Full Screen / Esc

Printer-friendly Version

Interactive Discussion



The weighting parameter $\alpha(\Delta z)$, is a measure of the proximity of overlap to maximum (exact when $\alpha(\Delta z) = 1$) or random (exact when $\alpha(\Delta z) = 0$); Negative values suggest some degree of minimum overlap (a combined cloud fraction greater than that of random overlap). A commonly used simplification, also adopted here, is that $\alpha(\Delta z)$ depends only on the separation distance Δz and not on the specific values of z_1 and z_2 , i.e., cloud fraction overlaps the exact same way at different heights of the atmosphere as long as Δz is the same. With this assumption, it was shown (Hogan and Illingworth, 2000) that $\alpha(\Delta z)$ can be fit reasonably well by an inverse exponential function:

$$\alpha(\Delta z) = \exp\left(-\frac{\Delta z}{L_\alpha}\right) \quad (4)$$

where L_α is the “decorrelation length” for cloud fraction overlap. Such a fit obviously does not allow for negative values $\alpha(\Delta z)$ which are occasionally observed (e.g., Oreopoulos and Norris, 2011). Because the fit provided by Eq. (4) is usually used in conjunction with Eq. (2), generalized overlap has also been termed “exponential-random” overlap (Hogan and Illingworth, 2000).

The manner in which cloud water contents align in the vertical may also important for processes like radiation (or precipitation). For example, the domain-averaged fluxes differ between a case where all high or low condensate values are aligned to create pockets of vertically integrated high or low water path (WP), and a case where a more random alignment homogenizes the WP horizontal distribution (e.g., see Norris et al., 2008). The nature of condensate alignment can be expressed in terms of rank correlations of water content as a function of separation distance $\Delta z = z_2 - z_1$ (e.g., see Pincus et al., 2005; Oreopoulos and Norris, 2011). For two layers at heights z_1 and z_2 the water contents at both heights can be ranked separately for the overlapping portion of N_{cld} subcolumns of the two cloud layers. A linear correlation coefficient $r(\Delta z)$ can

then be calculated from the ranks $R_i(z_1)$ and $R_i(z_2)$ according to:

$$r(\Delta z) = \frac{\sum_{i=1}^{N_{\text{cld}}} (R_i(z_1) - \bar{R}(z_1)) (R_i(z_2) - \bar{R}(z_2))}{\sqrt{\sum_{i=1}^{N_{\text{cld}}} (R_i(z_1) - \bar{R}(z_1))^2} \sqrt{\sum_{i=1}^{N_{\text{cld}}} (R_i(z_2) - \bar{R}(z_2))^2}} \quad (5)$$

The rank correlation coefficient expresses the likelihood water contents of the same relative strength within their respective layers are aligned in the vertical, with $r(z_1, z_2) = 1$ corresponding to perfect alignment and $r(z_1, z_2) = 0$ corresponding to completely random alignment.

It was suggested (e.g., Räisänen et al., 2004) that the rank correlation coefficient can also be fit by an inverse exponential (which again will not capture negative values) under similar assumptions as in the case of the cloud fraction overlap parameter, i.e., that it is only a function of Δz and not z itself

$$r(\Delta z) = \exp\left(-\frac{\Delta z}{L_r}\right) \quad (6)$$

where L_r is the rank correlation decorrelation length. Large values of L_r indicate condensate values that are highly correlated in terms of relative strength, while small values suggest condensate values whose relative strength is weakly correlated between layers.

The practical implementation of generalized cloud fraction overlap and condensate overlap using inverse exponential fits is described by Räisänen et al. (2004). The cloud generator that came with RRTMG could handle generalized cloud fraction overlap, but did not allow for overlap of condensate distributions; we added that feature following Räisänen et al. (2004). To create the subcolumns that describe the cloud fields within the GCM gridcolumns, two additional pieces of information, besides the profiles of cloud fraction C and mean condensate (liquid and ice) are needed, namely

Radiative impacts of cloud heterogeneity and overlap in an atmospheric GCM

L. Oreopoulos et al.

Title Page

Abstract

Introduction

Conclusions

References

Tables

Figures



Back

Close

Full Screen / Esc

Printer-friendly Version

Interactive Discussion



the decorrelation lengths L_α and L_r and the magnitude of the horizontal variability of the condensate distributions. We defer discussion of decorrelation lengths for the next section, and describe variability here.

To create condensate distributions for cloudy layers we assume that beta distributions describe the horizontal variations of normalized condensate $x = w/w_{\max}$:

$$\rho_\beta(x) = \frac{\Gamma(p+q)}{\Gamma(p)\Gamma(q)} x^{p-1} (1-x)^{q-1} \quad (7)$$

where Γ is the gamma function and the maximum value of condensate w_{\max} is set as five times the assumed variance σ_w^2 of the distribution. The shape parameters p , q of the beta distribution are calculated from the method of moments (Wilks, 1995):

$$p = \frac{\bar{x}^2(1-\bar{x})}{\sigma_x^2} - \bar{x} \quad (8a)$$

$$q = \frac{p(1-\bar{x})}{\bar{x}} \quad (8b)$$

where $\bar{x} = \bar{w}/w_{\max}$ and $\sigma_x^2 = \sigma_w^2/w_{\max}^2$.

The standard deviation σ_w of the distribution was set as follows, loosely based on Oreopoulos and Barker (1999) and our own analysis of hydrometeor variability in CloudSat (Stephens et al., 2002) data:

$$\begin{aligned} \sigma_w &= 0.5\bar{w} & \text{when } C > 0.99 \\ \sigma_w &= \bar{w}/\sqrt{2} & \text{when } 0.9 \leq C \leq 0.99 \\ \sigma_w &= \bar{w} & \text{when } C < 0.9 \end{aligned} \quad (9)$$

The choice of the beta distribution is supported by observations (Oreopoulos and Davies, 1998; Lee et al., 2010), but other skewed distributions that have also been observed from airborne and satellite measurements, such as gamma and lognormal

Radiative impacts of cloud heterogeneity and overlap in an atmospheric GCM

L. Oreopoulos et al.

Title Page

Abstract

Introduction

Conclusions

References

Tables

Figures

⏪

⏩

◀

▶

Back

Close

Full Screen / Esc

Printer-friendly Version

Interactive Discussion



and the CALIOP lidar of the CALIPSO mission (Winker et al., 2010), potentially allows a more detailed examination of spatiotemporal variation of cloud overlap decorrelation lengths.

We performed such a cloud overlap analysis using CloudSat products for two months, January and July 2009. For cloud fraction overlap we used the 2B-GEOPROF-LIDAR product which provides a cloud mask from combining the different hydrometeor detection capabilities of CPR and CALIOP (CPR is more capable at detecting layers with large concentrations of hydrometeors while CALIOP can better detect unobscured thin clouds). For condensate distribution overlap we use CloudSat's 2B-GEOPROF product which provides reflectivities for footprints (~ 1.7 km) that have been identified to contain hydrometeors at various vertical locations (separated by ~ 500 m). Our rank correlations according to Eq. (5) therefore actually come from reflectivities and not cloud condensates which are also available from CloudSat (e.g. product 2B-CWC-RO or 2B-CWC-RVOD), but are considered less reliable for the liquid phase due to drizzle and mixed/supercooled clouds often assigned erroneously to the ice phase (Lee et al., 2010). Since reflectivities are proportional to the size of the hydrometeor particles, under the assumption of constant particle number, the amount of condensate is monotonically related to particle size and Eq. (5) can be applied to reflectivities as well. A caveat of the 2B-GEOPROF reflectivities on the other hand is that they do not result only from interactions of the radar beam with suspended particles, but also precipitation particles. While the above make CloudSat-derived decorrelation lengths approximate, it should be kept in mind that the goal is not to obtain a perfect map of their geographical variation, but to have at our disposal a plausible general picture of their spatial and seasonal variability that can be contrasted with globally constant decorrelation lengths for cloud radiative effect studies.

Figure 1 shows the zonal distribution of L_α (top panel) and L_r (bottom panel) derived via least-square fits (Press et al., 1992) from monthly-averaged CloudSat/CALIPSO $\alpha(\Delta z)$ and $r(\Delta z)$ profiles within 3° latitude zones, for January and July (solid lines), with the limitations explained earlier. The data segment length used in the above calculation

Radiative impacts of cloud heterogeneity and overlap in an atmospheric GCM

L. Oreopoulos et al.

Title Page

Abstract

Introduction

Conclusions

References

Tables

Figures



Back

Close

Full Screen / Esc

Printer-friendly Version

Interactive Discussion



Radiative impacts of cloud heterogeneity and overlap in an atmospheric GCM

L. Oreopoulos et al.

Title Page

Abstract

Introduction

Conclusions

References

Tables

Figures

⏪

⏩

◀

▶

Back

Close

Full Screen / Esc

Printer-friendly Version

Interactive Discussion



is 100 CPR profiles (~ 170 km), similar to the spatial resolution of the AGCM experiments described below. There is a clear zonal structure for both months with tropical latitudes exhibiting larger decorrelation lengths (more maximum overlap and greater vertical alignment of reflectivities of similar relative strength), consistent with overlap contrasts between convective and stratiform regimes (Barker, 2008a,b; Oreopoulos and Norris, 2011). L_r values seem to be generally about half those of L_α , in broad agreement with previous findings (Räisänen et al., 2004; Pincus et al., 2005; Oreopoulos and Norris, 2011). Seasonal shifts of the peak values of decorrelation length appear to reflect the movement of the Intertropical Convergence Zone (ITCZ).

Our objective for AGCM parameterization purposes is to capture the observed decorrelation length zonal structure shown in Fig. 1. For that purpose, we apply a Gaussian fit (black dashed curves) of the form

$$L = m_1 + m_2 \exp \left[-(\theta - m_3)^2 / m_4^2 \right] \quad (10)$$

to the January (black) curves. In Eq. (10), θ is the latitude in degrees and m_1 , m_2 , m_3 and m_4 are parameter fits. All, except m_3 , are held constant, and their values yielding decorrelation length in km are provided in Table 1. Parameter m_3 , regulating the latitude at which Eq. (10) peaks, reflects the zonal movement seen in the CloudSat data, and is allowed to vary as a function of the day of the year according to:

$$m_3 = -4m_{3,0}(\text{jday} - 272)/365 \text{ when } \text{jday} > 181 \quad (11a)$$

$$m_3 = 4m_{3,0}(\text{jday} - 91)/365 \text{ when } \text{jday} \leq 181 \quad (11b)$$

where jday is the julian day. We set $m_{3,0} = 7.0$ (cloud fraction overlap) and $m_{3,0} = 8.5$ (condensate/reflectivity overlap). Our approach in essence consists of assigning the initial Gaussian fit of the monthly-averaged January observations to January 1, and then finding the zonally-averaged decorrelations for all other days of the year by applying Eqs. (10) and (11). This is the way the gray dashed curves in Fig. 1 (for 1 July) were derived. Note that the January fits describe the zonal distribution of both decorrelation lengths more realistically than the July curves which are not fits to the data, but

outcomes of the parameterization expressed by Eqs. (10) and (11); the parameterized northward shift of the January curves intended to capture July overlap generally leads to underestimates. Again, for the purposes of this study, where the goal is to examine the sensitivity of the cloud radiative effect to a range of decorrelation length specifications and the differences arising when the exact same overlap assumptions are applied to two different cloud schemes, we consider imperfect matching to observed overlap (itself coming with its own caveats) acceptable.

4.2 Description of AGCM experiments with diagnostic radiation

To examine the changes in the radiative impact of clouds when different assumptions are invoked about (a) the horizontal heterogeneity of their condensate; (b) the way their condensate distributions overlap; and (c) the way their cloud fractions overlap, relatively short (~ 1 yr) simulations with the GEOS-5 AGCM are conducted with RRTMG producing “diagnostic” only fluxes. Had we wanted to examine the full impact of our cloud changes on the model climate much longer simulations of at least a decade with interactive RRTMG would have been necessary. By diagnostic RRTMG radiation fields we mean that the heating and cooling rates produced by the RRTMG calculations are not supplied back to the AGCM to affect dynamical and physical processes. Instead, the model run is driven by the radiation fields of the original (operational) radiation package (Chou and Suarez, 1999; Chou et al., 2001) which treats clouds according to its default configuration, as usual. The McICA configuration of RRTMG simply runs side-by-side with the original radiation package and operates on the cloud fields produced by the standard model, but as transformed by the cloud generator in accordance with our heterogeneity and overlap assumptions.

Our suite of experiments is summarized in Table 2. All experiments were run with the GEOS-5 AGCM Fortuna 2.5 at $2 \times 2.5^\circ$ resolution with 72 vertical levels, and differ only in their assumptions about the cloud fields. While all experiments share the same profiles of cloud fraction and mean condensate, other assumptions about the nature of the clouds are different from experiment to experiment. Clouds can be assumed

Radiative impacts of cloud heterogeneity and overlap in an atmospheric GCM

L. Oreopoulos et al.

Title Page

Abstract

Introduction

Conclusions

References

Tables

Figures



Back

Close

Full Screen / Esc

Printer-friendly Version

Interactive Discussion



Radiative impacts of cloud heterogeneity and overlap in an atmospheric GCM

L. Oreopoulos et al.

Title Page

Abstract

Introduction

Conclusions

References

Tables

Figures

⏪

⏩

◀

▶

Back

Close

Full Screen / Esc

Printer-friendly Version

Interactive Discussion



to be horizontally homogeneous or heterogeneous and their cloud fractions can overlap according to either the maximum-random or generalized overlap paradigms. When clouds are heterogeneous and overlap according to the maximum-random overlap assumption, a condensate decorrelation length still needs to be supplied. All simulations correspond to 13-month runs from which the last 12 months are considered for analysis; prescribed sea surface temperatures for the period May 1993 to May 1994 are used.

Two sets of experiments were conducted. One where the standard (control) cloud scheme (Molod et al., 2012) operates and one with McRAS-AC (Sud et al., 2012; Sud and Lee, 2007). The two cloud schemes share the same convective scheme (RAS), but with different assumptions about the onset of convection, and ambient air entrainment (quadratic in McRAS versus linear in standard RAS) and are fundamentally different in their stratiform cloud parameterizations and microphysics descriptions. The control cloud scheme has pre-specified liquid and ice particle sizes, while McRAS-AC has active cloud microphysics where condensate amounts, particle sizes, and precipitation depend on the aerosol loading. For our experiments we chose to provide McRAS-AC with a present day climatology of aerosol mass concentrations produced by the GO-CART (Chin et al., 2000) chemical transport model. Note that for both sets of experiments, while the aerosols are radiatively active in the operational radiation package that provides interactive radiation fields, they are not considered in RRTMG which produces the diagnostic radiation fields used to assess overlap impacts on CRE.

For each of the experiments we generate the monthly, seasonal and annual geographical distribution of the LW and SW cloud radiative effect (CRE) at the top of the atmosphere (TOA). The CRE is defined as:

$$CRE_{LW,SW} = F_{LW,SW}^{clr} - F_{LW,SW}^{cl} \quad (12a)$$

which can also be written as

$$CRE_{LW,SW} = C_{tot} (F_{LW,SW}^{clr} - F_{LW,SW}^{ovc}) \quad (12b)$$

Radiative impacts of cloud heterogeneity and overlap in an atmospheric GCM

L. Oreopoulos et al.

Title Page

Abstract

Introduction

Conclusions

References

Tables

Figures

⏪

⏩

◀

▶

Back

Close

Full Screen / Esc

Printer-friendly Version

Interactive Discussion



where F is the outgoing flux (LW or SW) at the TOA, *clr* designates clear (cloudless) skies, *cld* a mixture of clear and cloudy skies, and *ovc* overcast skies (100% cloud fraction); C_{tot} is the total vertically projected cloud fraction. The modeled CRE always comes from Eq. (12a); nevertheless, Eq. (12b) which applies when the cloudy sky flux can be written as the linear combination of clear and overcast fluxes, can be used for interpreting the CRE, since a gridcolumn's C_{tot} is not uniquely defined, but rather depends on the cloud fraction overlap assumption (for the same cloud fraction profile, the closer the overlap to random, the larger C_{tot} ¹). For the complete intercomparison of CRE among all experiments we use globally-averaged values. For select experiments we also compare zonal (latitudinal) averages and geographical distributions. Although not important for understanding the sensitivity of CRE to cloud heterogeneity and overlap, we also include in our comparison TOA CRE from the CERES EBAF v. 2.6 data set (Loeb et al., 2009) for the period March 2000 to June 2011.

5 Analysis of cloud radiative effect dependencies

5.1 Global changes in CRE

We first focus on the sensitivity of globally-averaged CRE to different assumptions about how cloud fields can be generated from profiles of cloud fraction and mean condensate. Figures 2 and 3 chart this sensitivity for the control (CTL) and McRAS-AC cloud schemes, respectively. The center box contains AGCM results for the “default” (reference) configuration, namely homogeneous condensate distributions and maximum-random cloud fraction overlap (Exp. 1, see Table 2). Blue numbers depict CRE_{LW} and red CRE_{SW} values. This box also contains the observed global CREs according to the CERES EBAF (Loeb et al., 2009) product. The numbers in parentheses show the difference between the AGCM with default cloud configuration and observed

¹Minimum overlap of various degrees produces even larger C_{tot} , but there is no such overlap in our experiments.

Radiative impacts of cloud heterogeneity and overlap in an atmospheric GCM

L. Oreopoulos et al.

[Title Page](#)

[Abstract](#)

[Introduction](#)

[Conclusions](#)

[References](#)

[Tables](#)

[Figures](#)

[⏪](#)

[⏩](#)

[◀](#)

[▶](#)

[Back](#)

[Close](#)

[Full Screen / Esc](#)

[Printer-friendly Version](#)

[Interactive Discussion](#)

CRE (reference model-observations). Because CRE_{LW} is a positive quantity, model underestimates yield negative differences, while the opposite is true for CRE_{SW} which is a negative quantity. The other boxes show how much the CRE differs from the reference model results in the center box when assumptions about the nature of the cloud fields change, i.e., reference (= max-ran homogenous) minus other experiments. For example, when keeping the cloud fraction overlap maximum-random, but allowing the clouds to be inhomogeneous according to Eqs. (7)–(9) (leftmost box, corresponding to Exp. 2), CRE_{LW} decreases by 2.3 W m^{-2} (+2.3) and CRE_{SW} also decreases in absolute value (i.e., a smaller negative value) by 5.6 W m^{-2} (–5.6). When keeping clouds homogeneous but changing the cloud fraction overlap to generalized (with globally constant $L_\alpha = 2 \text{ km}$, Exp. 3), CRE_{LW} increases by 4.3 W m^{-2} (–4.3), and CRE_{SW} also increases in absolute terms by 4.3 W m^{-2} (+4.3) (box 3). Therefore, because of the conventions we have adopted for reporting our results, and the sign of the CRE arising from Eq. (12) (positive for LW, negative for SW), increases in CRE_{LW} (stronger LW radiative effect) appear as negative numbers in the boxes of Figs. 2 and 3, while increases in CRE_{SW} (stronger SW radiative effect) appear as positive numbers. When the sign of the differences is reversed, the interpretation changes accordingly, i.e., positive CRE_{LW} differences signify weaker LW radiative effect, while negative CRE_{SW} differences also signify weaker SW radiative effect.

Having clarified the sign conventions of our CRE differences, we now proceed to the physical interpretation of the results. We start with Fig. 2 which refers to the CTL cloud scheme. Introducing heterogeneity (inhomogeneity) in the condensate distributions following Eqs. (7)–(9) reduces the strength of CRE (box 2, corresponding to Exp. 2 on the left). This is because for the same mean condensate, heterogeneous clouds reflect less solar radiation (e.g., Cahalan et al., 1994) and emit less (transmit more) LW radiation (Barker and Wielicki, 1997). For this particular case therefore changes in CRE can be attributed to changes in $F_{LW,SW}^{ovc}$ in Eq. (12b): the SW outgoing flux for overcast conditions goes down, while the LW outgoing radiation goes up; in both cases the contrast with the clear-sky flux is reduced. The change in CRE_{SW} is more than

Radiative impacts of cloud heterogeneity and overlap in an atmospheric GCM

L. Oreopoulos et al.

Title Page

Abstract

Introduction

Conclusions

References

Tables

Figures

⏪

⏩

◀

▶

Back

Close

Full Screen / Esc

Printer-friendly Version

Interactive Discussion



double that on CRE_{LW} since the nonlinearity of the LW emittance curve is restricted to a much narrower range of cloud condensates (or, strictly speaking, optical depths) than the nonlinearity of the SW albedo curve. In other words, changes in the details of an optical depth distribution begin to matter less (because of saturation in emittance) at lower values of mean cloud optical depth. When cloud distributions remain homogeneous, on the other hand, but cloud fraction overlap changes (transition from box 1 to box 3), it is C_{tot} in Eq. (12b) that is mainly affected (it appears from our results that the change in the distribution of cloud tops exposed to space, which matters for the LW, is a lesser contributor). Both CRE_{SW} and CRE_{LW} become stronger by the same magnitude (4.3 W m^{-2}), indicating that for the CTL cloud scheme C_{tot} for generalized overlap is higher than that for maximum-random overlap.

When condensate heterogeneity is applied under conditions of generalized overlap (Exp. 4, lower right box), the effect of increased C_{tot} in the CTL cloud scheme is entirely cancelled out for CRE_{SW} through decrease in F_{SW}^{ovc} , and partially cancelled out for CRE_{LW} through increase in F_{LW}^{ovc} . The end result is that CRE_{SW} is weaker by 2 W m^{-2} compared to the reference Exp. 1, while CRE_{LW} remains stronger than in Exp. 1, but by only 1.3 W m^{-2} . Note that the effect of inhomogeneity on CRE is stronger when cloud fraction obeys generalized overlap (from Exp. 3 to Exp. 4) than when it obeys maximum-random overlap (from Exp. 1 to Exp. 2): in the former case CRE_{SW} and CRE_{LW} decrease in strength by 6.3 W m^{-2} and 3 W m^{-2} , respectively, while for the latter case they decrease by 5.6 W m^{-2} and 2.3 W m^{-2} . When the standard deviation used for the beta distribution of condensate is halved compared to Eq. (9) (box 5), CRE_{SW} is reduced by about 2 W m^{-2} , while CRE_{LW} is reduced by 1 W m^{-2} reflecting again the fact that any changes that affect overcast fluxes instead of cloud fractions have greater impact on the SW compared to the LW.

A simultaneous change in both cloud fraction and condensate overlap can be achieved by switching from globally constant decorrelation lengths to CloudSat-based decorrelation lengths (Eqs. 10–11 and Fig. 1). This process is represented by the transition from Exp. 4 to Exp. 8 shown by the bottom two boxes (4 and 8) of Fig. 2.

Radiative impacts of cloud heterogeneity and overlap in an atmospheric GCM

L. Oreopoulos et al.

Title Page

Abstract

Introduction

Conclusions

References

Tables

Figures

⏪

⏩

◀

▶

Back

Close

Full Screen / Esc

Printer-friendly Version

Interactive Discussion

CRE_{SW} strength decreases by 1 W m^{-2} , while CRE_{LW} decreases by 0.7 W m^{-2} . Recall that the numbers in the boxes show differences with respect to the reference Exp. 1 represented by the center box (box 1), so one can see that transitioning from homogeneous maximum-random overlap to inhomogeneous clouds following a CloudSat-based generalized overlap results in 3 W m^{-2} weaker CRE_{SW}, but a slightly stronger (by 0.6 W m^{-2}) CRE_{LW}. This is possible because while cloud fraction changes (from maximum-random to generalized) have about the same effect on both the SW and LW CRE, overcast flux changes (from condensate overlap and inhomogeneity) are too weak in the LW to reverse the increased CRE of generalized overlap.

The CRE response to condensate heterogeneity and generalized overlap when imposed on the cloud fields of an alternate cloud scheme can be substantially different than the one discussed above. This is shown in Fig. 3, which is the same as Fig. 2, but for the McRAS-AC cloud scheme. Cloud water inhomogeneity under conditions of maximum-random cloud fraction overlap (box 2) results in a slightly smaller weakening of CRE_{SW}, and a slightly greater weakening of CRE_{LW}. The transition of homogeneous clouds from maximum-random overlap to generalized overlap (box 3) gives a much smaller CRE response for McRAS-AC ($\sim 1 \text{ W m}^{-2}$ compared to $\sim 4 \text{ W m}^{-2}$ for CTL). Adding inhomogeneity to clouds obeying generalized overlap has about the same CRE effect for McRAS-AC as adding inhomogeneity to clouds following maximum-random overlap (CRE changes from Exp. 3 to Exp. 4 are about the same as the changes from Exp. 1 to Exp. 2); for the CTL cloud scheme the CRE impacts diverged by 0.7 W m^{-2} . The box corresponding to Exp. 5 indicates that when the imposed inhomogeneity is reduced by half on clouds following generalized overlap, the outcome is close to the reference CRE values, i.e., the effects of modified overlap and inhomogeneity largely cancel out; this was not the case for the CTL cloud scheme for which overlap had a much stronger CRE impact than reduced inhomogeneity. Finally, the change from globally constant decorrelation lengths to zonally-dependent decorrelation lengths (Exp. 4 to Exp. 8) is notably smaller for the McRAS-AC cloud fields compared to the CTL cloud scheme.

Radiative impacts of cloud heterogeneity and overlap in an atmospheric GCM

L. Oreopoulos et al.

Title Page

Abstract

Introduction

Conclusions

References

Tables

Figures

⏪

⏩

◀

▶

Back

Close

Full Screen / Esc

Printer-friendly Version

Interactive Discussion



This latter result is also included in Fig. 4 which adopts the conventions of Figs. 2 and 3, but focuses on CRE changes brought by changing the parameters (i.e., decorrelation lengths) of generalized overlap. The left part of the figure provides global CRE impacts for the CTL cloud scheme while the right part of the figure does the same for the McRAS-AC scheme. In this figure the reference CREs come from Exp. 4 (heterogeneous clouds, generalized overlap with constant decorrelation lengths), upper left box (box 4); all other boxes contain CRE differences from these reference CREs using the sign conventions of Figs. 2 and 3. The transition from Exp. 4 to Exp. 7 (top boxes 4 and 7) captures the effect of changing the condensate overlap decorrelation length L_r . When it is doubled from 1 to 2 km both CRE_{SW} and CRE_{LW} decrease in strength slightly. This is the result of more aligned condensate distributions increasing the variability in integrated WP compared to shorter L_r (more random overlap of layer condensate distributions producing more homogeneous WP distributions) and consequently yielding reduced TOA F_{SW}^{ovc} and increased F_{LW}^{ovc} . If the global decorrelation length of cloud fraction L_α is doubled from 2 to 4 km (transition from Exp. 7 to Exp. 6, right boxes) the reduced C_{tot} of less random overlap yields further reductions of 3 W m^{-2} and 1.8 W m^{-2} in CRE_{SW} and CRE_{LW} , respectively. Because the observed decorrelation lengths are generally smaller than those of Exp. 6, when they are applied in the cloud generator (transition from Exp. 6 to Exp. 8, bottom boxes) the CREs increase again (higher C_{tot} and more homogeneous distributions of WP) and become comparable to those of Exp. 7. For the CTL cloud scheme, the overall impact of using CloudSat-based decorrelation lengths instead of global values of $L_\alpha = 2 \text{ km}$ and $L_r = 1 \text{ km}$ (Exp. 4 to Exp. 8., left boxes) is about 1 W m^{-2} , slightly more for CRE_{SW} and slightly less for CRE_{LW} . These differences are at first glance too small to justify the effort of deriving zonally-dependent decorrelation lengths, especially since the Exp. 4 CREs are already below CERES EBAF and the more sophisticated treatment of overlap makes the discrepancy from observed CREs worse. But as will be shown below, the rather benign global CRE changes hide local impacts that are much more substantial.

The right part of Fig. 4 contains the exact same analysis as the left part, but for the McRAS-AC scheme implemented in GEOS-5. The impact of doubling the rank correlation decorrelation length (Exp. 4 to Exp. 7) is about the same as for CTL, but doubling the overlap decorrelation length does not change CRE as much for McRAS-AC. The Exp. 6 and Exp. 4 to Exp. 8 transitions are also weaker in terms of CRE changes for McRAS-AC. When these results are considered in conjunction with Fig. 3, the obvious conclusion is that McRAS-AC clouds do not cause as big CRE changes as CTL clouds in response to the different prescriptions of cloud overlap. We will explain why this is so in Sect. 5.3.

As a concluding thought we would like to point out that if CRE_{SW} is overestimated and CRE_{LW} underestimated compared to observations, as is the case for the CTL cloud scheme, it is not possible to bring both simultaneously closer to observations through changes in inhomogeneity and overlap descriptions alone. Inhomogeneity reduces CRE_{SW} and can bring model and observations closer, but it also reduces the already too low CRE_{LW} . Similarly, increasing CRE_{LW} via changes in overlap (i.e., increasing C_{tot}) to match observations has the undesired effect of making the CRE_{SW} overestimates worse. To match both components of CRE to observations, inhomogeneity and overlap changes should be accompanied by changes in other cloud properties such as cloud top height and mean condensate as well.

5.2 Geographical changes in CRE

In this section we examine whether the relatively narrow range of global CRE impact due to changes in cloud overlap specification conceals a much wider range of regional CRE changes. For the sake of brevity, we focus on only two overlap specification changes, the transition from maximum-random overlap to generalized overlap with globally constant decorrelation lengths (with heterogeneous clouds), and the transition from the latter type of overlap to generalized overlap with zonally variable decorrelation lengths as parameterized per the CloudSat data analysis. In other words we examine regional CRE changes between Exp. 2 and Exp. 4 and between Exp. 8 and Exp. 4.

Radiative impacts of cloud heterogeneity and overlap in an atmospheric GCM

L. Oreopoulos et al.

Title Page

Abstract

Introduction

Conclusions

References

Tables

Figures



Back

Close

Full Screen / Esc

Printer-friendly Version

Interactive Discussion



Radiative impacts of cloud heterogeneity and overlap in an atmospheric GCM

L. Oreopoulos et al.

[Title Page](#)

[Abstract](#)

[Introduction](#)

[Conclusions](#)

[References](#)

[Tables](#)

[Figures](#)

[⏪](#)

[⏩](#)

[◀](#)

[▶](#)

[Back](#)

[Close](#)

[Full Screen / Esc](#)

[Printer-friendly Version](#)

[Interactive Discussion](#)



Figure 5 shows maps of annually averaged CRE_{SW} differences between the experiments mentioned above, while Fig. 6 is a counterpart figure for CRE_{LW} . The panels in the top row correspond to Exp. 2 minus Exp. 4 differences, and the panels in the bottom row to Exp. 8 minus Exp. 4 differences; the left panels are for the CTL cloud scheme and the right panels for McRAS-AC. The CTL cloud scheme yields substantially greater CRE differences for the transition from maximum-random to generalized overlap than between two generalized overlaps, and in the tropics compared to midlatitudes. Zonal CRE differences between Exp. 2 and Exp. 4 peak at $\sim 11 \text{ W m}^{-2}$ in the SW and $\sim -10 \text{ W m}^{-2}$ in the LW around 5° N (left panels of Fig. 7) reflecting changes in C_{tot} of ~ 0.13 (blue curve in the top panel of Fig. 8). The counterpart CRE differences between Exp. 8 and Exp. 4 are $\sim 6 \text{ W m}^{-2}$ and $\sim -4 \text{ W m}^{-2}$ for a C_{tot} change of about 0.05 (red curve in the top panel of Fig. 8); in this case however the different vertical alignment of condensate distributions also contributes to the CRE differences, making the CRE_{SW} and CRE_{LW} changes more distinct. It is interesting that the sign of the CRE differences between Exp. 8 and Exp. 4 (changes in the details of generalized overlap) is not the same everywhere. While the CRE_{SW} (CRE_{LW}) difference is generally positive (negative), at midlatitudes there are negative (positive) differences with peaks at about 60° latitude. The difference in behaviour from tropics to midlatitudes is solely due the parameterization of the CloudSat-based decorrelation lengths of Fig. 1. The constant decorrelation lengths are lower than those from CloudSat in the tropics and yield higher C_{tot} and more homogenous WPs, ergo, stronger CRE (expressed as positive CRE_{SW} and negative CRE_{LW} differences). In the midlatitudes on the other hand, the opposite is true, i.e., the globally constant values are above the CloudSat-based parameterized decorrelation lengths resulting in weaker CREs for Exp. 4 compared to Exp. 8 (negative CRE_{SW} and positive CRE_{LW} differences).

The counterpart McRAS-AC CRE differences are much weaker, as can be seen in the right panels of Figs. 5, 6, and 7, consistent with much smaller changes in C_{tot} (Fig. 8) and the smaller global CRE differences noted earlier in Figs. 3 and 4. The zonal structure of the Exp. 8 minus Exp. 4 CRE differences can be explained by invoking the

same arguments as earlier for the CTL cloud scheme, but exhibit notably smaller values. The Exp. 2 minus Exp. 4 CRE differences also have the same sign as in CTL across all latitudes, but exhibit a much weaker latitudinal dependence without the tropical peak of CTL, while being also substantially smaller. One interesting feature seen in the bottom panel of Fig. 8 is that the zonally-averaged C_{tot} difference for Exp. 2 minus Exp. 4 is not only small, but generally positive, in contrast to CTL. This means that either generalized overlap consistently results in slightly smaller total cloud fractions than maximum-random overlap, or that the instances where C_{tot} from maximum-random overlap is greater exceeds those where the reverse is true. This in turn points to cloud vertical profiles in McRAS-AC where the random part (cloudy layers separated by clear layers) of maximum-random overlap is invoked more often than in CTL. Recall that within the confines of generalized overlap, exact random cloud fraction overlap can only occur in the limit of an infinitely large decorrelation length.

5.3 Why overlap details in the two cloud schemes affect CRE differently

The quite distinct CRE response of the two cloud schemes when the cloud generator is furnished with identical rules to produce cloudy subcolumns from the same profiles of cloud fraction and mean condensate for radiation calculations, merits further examination. Since the largest impact comes from the overlap of cloud fraction, we examine here how the two schemes differ in terms of cloud fraction means and distributions, and in their frequency of multi-layer cloud occurrences.

First we examine the one-year cloud fraction climatology produced by the two schemes. We compare in Fig. 9 annually- and zonally-averaged cloud fraction profiles produced by CTL (top) and McRAS-AC (bottom). The differences between the two panels are striking. McRAS-AC produces in general larger cloud fractions throughout the entire extent of the midlatitude and polar troposphere and the largest part of the tropical troposphere. The CTL cloud scheme on the other hand produces higher cloud fractions in areas of tropical deep convection, and exhibits some cloud presence at the higher altitudes of the midlatitude atmosphere where McRAS-AC produces no clouds.

Radiative impacts of cloud heterogeneity and overlap in an atmospheric GCM

L. Oreopoulos et al.

Title Page

Abstract

Introduction

Conclusions

References

Tables

Figures



Back

Close

Full Screen / Esc

Printer-friendly Version

Interactive Discussion



Radiative impacts of cloud heterogeneity and overlap in an atmospheric GCM

L. Oreopoulos et al.

[Title Page](#)[Abstract](#)[Introduction](#)[Conclusions](#)[References](#)[Tables](#)[Figures](#)[Back](#)[Close](#)[Full Screen / Esc](#)[Printer-friendly Version](#)[Interactive Discussion](#)

The natural outcome of these average cloud fraction profiles is that C_{tot} is higher for the McRAS-AC cloud scheme. This is clearly demonstrated in the Fig. 10 zonal plot showing C_{tot} from Exp. 2 (maximum-random overlap) and Exp. 4 (generalized overlap with $L_{\alpha} = 2\text{km}$) which makes apparent that McRAS-AC produces higher zonal cloud fractions everywhere for Exp. 2 and nearly everywhere (except a portion of the tropics) for Exp. 4. The higher cloud fractions for McRAS-AC come with much greater insensitivity to the overlap specification (the distance between the blue and red curves, also shown as difference in Fig. 8). Indeed, larger cloud fractions make the details of overlap more inconsequential since the difference between maximum, random and any degree in between (i.e., generalized), becomes smaller at the high end of the cloud fraction distribution.

A better way to demonstrate the tendency of McRAS-AC to produce higher cloud fractions is to examine instantaneous layer cloud fractions. We produced distributions for this quantity for both cloud schemes from twice-daily samples extracted during January and July within the period of our runs. The four distributions are shown in Fig. 11. The seasonal differences are not pronounced, especially for McRAS-AC, but the differences between the two cloud schemes is striking. McRAS-AC generates many more layer cloud fractions in the 0.5–0.9 range, and also produces overcast cloud layers which the CTL scheme never does. The smaller zonal averages of total cloud fraction by the CTL cloud scheme in Fig. 10 appear therefore to be the result of consistently lower than McRAS-AC occurrences of instantaneous layer cloud fractions above 0.5.

Another factor that makes the details of overlap specification matter less is the number of cloudy layer within a gridcolumn at a particular instance. The more layers are cloudy, the greater the chance that they will be farther apart and therefore the greater the tendency towards random overlap conditions either under maximum-random overlap or generalized overlap. In this regard, McRAS-AC is again distinct from CTL in producing more occurrences of large numbers of model layers that are simultaneously cloudy (Fig. 12) within the gridcolumn at a particular instance.

All the above results portray a consistent picture: McRAS-AC is more cloudy than CTL under a variety of metrics and high cloud fractions are produced frequently enough to make the exact overlap specification less influential on C_{tot} and CRE.

6 Discussion and conclusions

5 While earlier studies have shown that vertical cloud structure and particularly cloud fraction overlap can have large instantaneous effects, especially on solar fluxes (Barker et al., 1999), global effects within climate models have been less systematically quantified. Recent progress due to new capabilities in describing within GCMs arbitrary cloud fraction and condensate overlaps that resemble more faithfully the vertical cloud structures observed in nature, along with progress on how radiation schemes can handle these more complex cloud fields, will help ameliorate the current state of affairs. Our study contributes to this need by attempting to address the following question: do the details of cloud overlap matter radiatively to a similar extent when applied the exact same way on the (different) mean cloud fraction and condensate fields produced by two distinct cloud schemes? The answer is negative; we find one cloud scheme producing cloud distributions which after overlap manipulation can change the radiative fluxes much more than another cloud scheme. This means that there is no definitive answer on whether the details of cloud vertical structure matter much for radiation: it will depend on the host model and/or its cloud scheme. In contrast, introducing cloud condensate heterogeneity is found to matter more consistently across cloud schemes while the details of how the inhomogeneous distributions overlap in the vertical has only a small impact.

20 The radiative consequences of cloud vertical structure and condensate heterogeneity were studied in this paper diagnostically, in other words, changes in radiation brought about by these factors did not feed back to the model (a separate radiation scheme blind to our changes of cloud vertical correlations was running for that purpose). In that sense, our study resembles that of Shonk and Hogan (2010) who

Radiative impacts of cloud heterogeneity and overlap in an atmospheric GCM

L. Oreopoulos et al.

Title Page

Abstract

Introduction

Conclusions

References

Tables

Figures



Back

Close

Full Screen / Esc

Printer-friendly Version

Interactive Discussion



Radiative impacts of cloud heterogeneity and overlap in an atmospheric GCM

L. Oreopoulos et al.

Title Page

Abstract

Introduction

Conclusions

References

Tables

Figures



Back

Close

Full Screen / Esc

Printer-friendly Version

Interactive Discussion



examined the radiative impact of different assumptions about condensate horizontal variability and cloud overlap by operating on cloud fields from re-analysis data. In that study the global effects of cloud fraction overlap (their “vertical shift”) on SW and LW CRE were (absolute values) $\sim 4 \text{ W m}^{-2}$ and $\sim 2 \text{ W m}^{-2}$. The experiment transition from which these numbers were obtained are roughly equivalent to our transitions from Exp. 2 to Exp. 4 (see Figs. 2 and 3). In our case the change in CRE is $\sim 3.6 \text{ W m}^{-2}$ for both the SW and LW in the CTL cloud scheme; the alternate McRAS-AC cloud scheme produces CRE changes slightly below 1 W m^{-2} . We conclude that studies of this type may eventually put an upper limit on the global impact of cloud overlap in current large scale models, but with a range of outcomes that may remain quite wide. Even greater variability range is expected to occur at smaller spatial scales. Our zonal average peak CRE impact is $\sim 10 \text{ W m}^{-2}$, for both SW and LW CRE while that of Shonk and Hogan (2010) reaches such values (with much less zonal structure) only in the SW; the LW peak is about half, consistent with their global result.

We did not discuss much the level of agreement of simulated CRE for our different experiments with observed CRE. This was a conscious decision since agreement, at global levels at least, can be achieved through appropriate tuning. Figures 2 and 3 show that the best agreement is not necessarily obtained with the most realistic assumptions about the nature of the cloud fields. Nevertheless, it should be noted that if one of the CRE components is overestimated and the other underestimated, both cannot be simultaneously pushed towards observations by adjustments to cloud condensate heterogeneity and overlap alone. This is because any change that strengthens one component of CRE will have the undesired effect of doing the same for the other component as well.

Acknowledgement. The authors gratefully acknowledge support by the NASA Modeling Analysis and Prediction and CloudSat/CALIPSO Science Team Recompete programs managed by David Conidine. Computational resources and support were provided from the NASA Center for Climate Simulation (NCCS). We would also like to thank M. Iacono and E. Mlawer of AER for their assistance in implementing RRTMG into GEOS-5.

References

- Barker, H. W.: Overlap of fractional cloud for radiation calculations in GCMs: a global analysis using CloudSat and CALIPSO data, *J. Geophys. Res.*, 113, D00A01, doi:10.1029/2007JD009677, 2008a.
- 5 Barker, H. W.: Representing cloud overlap with an effective decorrelation length: an assessment using CloudSat and CALIPSO data, *J. Geophys. Res.*, 113, D24205, doi:10.1029/2008JD010391, 2008b.
- Barker, H. W. and Wielicki, B. A.: Parameterizing grid-averaged longwave fluxes for inhomogeneous marine boundary layer clouds, *J. Atmos. Sci.*, 54, 2785–2798, 1997.
- 10 Barker, H. W., Stephens, G. L., and Fu, Q.: The sensitivity of domain-averaged solar fluxes to assumptions about cloud geometry, *Quart. J. Roy. Meteor. Soc.*, 125, 2127–2152, 1999.
- Barker, H. W., Cole, J. N. S., Morcrette, J.-J., Pincus, R., Räisänen, P., von Salzen, K., and Vaillancourt, P. A.: The Monte Carlo independent column approximation: an assessment using several global atmospheric models, *Q. J. R. Met. Soc.*, 134, 1463–1478, 2008.
- 15 Chin, M., Rood, R. B., Lin, S.-J., Muller, J.-F., and Thompson, A. M.: Atmospheric sulfur cycle simulated in the global model GOCART: model description and global properties, *J. Geophys. Res.*, 105, 24671–24687, 2000.
- Chou, M.-D. and Suarez, M. J.: A solar radiation parameterization for atmospheric studies, Technical Report Series on Global Modeling and Data Assimilation, NASA/TM-1999-10460, 15, 52 pp., 1999.
- 20 Chou, M.-D., Suarez, M. J., Liang, X.-Z., and Yan, M. H.: A thermal infrared radiation parameterization for atmospheric studies, Technical Report Series on Global Modeling and Data Assimilation, NASA/TM-2001-104606, 19, 65 pp., 2001.
- Clough, S. A., Shephard, M. W., Mlawer, E. J., Delamere, J. S., Iacono, M. J., Cady-Pereira, K., Boukabara, S., and Brown, P. D.: Atmospheric radiative transfer modeling: a summary of the AER codes, *J. Quant. Spectrosc. Radiat. Transfer*, 91, 233–244, 2005.
- 25 Geleyn, J. F. and Hollingsworth, A.: An economical analytical method for the computation of the interaction between scattering and line absorption of radiation, *Contrib. Atmos. Phys.*, 52, 1–16, 1979.
- 30 Hogan, R. J. and Illingworth, A. J.: Deriving cloud overlap statistics from radar, *Q. J. R. Meteor. Soc.*, 126, 2903–2909, 2000.

Radiative impacts of cloud heterogeneity and overlap in an atmospheric GCM

L. Oreopoulos et al.

Title Page

Abstract

Introduction

Conclusions

References

Tables

Figures



Back

Close

Full Screen / Esc

Printer-friendly Version

Interactive Discussion



Radiative impacts of cloud heterogeneity and overlap in an atmospheric GCM

L. Oreopoulos et al.

Title Page

Abstract

Introduction

Conclusions

References

Tables

Figures

⏪

⏩

◀

▶

Back

Close

Full Screen / Esc

Printer-friendly Version

Interactive Discussion



- Hogan, R. J. and Illingworth, A. J.: Parameterizing ice cloud inhomogeneity and the overlap of inhomogeneities using cloud radar data, *J. Atmos. Sci.*, 60, 756–767, 2003.
- Iacono, M. J., Delamere, J. S., Mlawer, E. J., Shephard, M. W., Clough, S. A., and Collins, W. D.: Radiative forcing by long-lived greenhouse gases: calculations with the AER radiative transfer models, *J. Geophys. Res.*, 113, D13103, doi:10.1029/2008JD009944, 2008.
- Lacis, A. A. and Oinas, V.: A description of the correlated k distribution method for modeling nongray gaseous absorption, thermal emission, and multiple scattering in vertically inhomogeneous atmospheres, *J. Geophys. Res.*, 96, 9027–9063, 1991.
- Lee, S., Kahn, B. H., and Teixeira, J.: Characterization of cloud liquid water content distributions from CloudSat, *J. Geophys. Res.*, 115, D20203, doi:10.1029/2009JD013272, 2010.
- Loeb, N. G., Wielicki, B., Doelling, D., Smith, G., Keyes, D., Kato, S., Manalo-Smith, N., and Wong, T.: Toward optimal closure of the earth's top-of-atmosphere radiation budget, *J. Climate*, 22, 748–766, 2009.
- Mace, G. G. and Benson-Troth, S.: Cloud layer overlap characteristics derived from long-term cloud radar data, *J. Climate*, 15, 2505–2515, 2002.
- Mlawer, E. J., Taubman, S. J., Brown, P. D., Iacono, M. J., and Clough, S. A.: RRTM, a validated correlated-*k* model for the longwave, *J. Geophys. Res.*, 102, 16663–16682, 1997.
- Molod, A., Takacs, L., Suarez, M. J., Bacmeister, J., Song, I.-S., Eichmann, A., and Chang, Y.: The GEOS-5 atmospheric General Circulation Model: mean climate and development from MERRA to Fortuna, NASA, Technical Report Series on Global Modeling and Data Assimilation, NASA/TM-2008-104606, 28, 112 pp., 2012.
- Morcrette, J. J., Barker, H. W., Cole, J. N. S., Iacono, M. J., and Pincus, R.: Impact of a new radiation package, McRad, in the ECMWF integrated forecasting system, *Mon. Wea. Rev.*, 136, 4773–4798, 2008.
- Naud, C. M., Del Genio, A., Mace, G. G., Benson, S., Clothiaux, E. E., and Kollias, P.: Impact of dynamics and atmospheric state on cloud vertical overlap, *J. Climate*, 21, 1758–1770, doi:10.1175/2007JCLI1828.1, 2008.
- Norris, P. M., Oreopoulos, L., Hou, A. Y., Tao, W. K., and Zeng, X.: Representation of 3-D heterogeneous cloud fields using copulas: theory for water clouds, *Q. J. R. Meteorol. Soc.*, 134, 1843–1864, 2008.
- Oreopoulos, L. and Barker, H. W.: Accounting or subgrid-scale cloud variability in a multi-layer 1D solar radiative transfer algorithm, *Q. J. R. Meteorol. Soc.*, 125, 301–330, 1999.

Radiative impacts of cloud heterogeneity and overlap in an atmospheric GCM

L. Oreopoulos et al.

[Title Page](#)

[Abstract](#)

[Introduction](#)

[Conclusions](#)

[References](#)

[Tables](#)

[Figures](#)

[⏪](#)

[⏩](#)

[◀](#)

[▶](#)

[Back](#)

[Close](#)

[Full Screen / Esc](#)

[Printer-friendly Version](#)

[Interactive Discussion](#)



- Oreopoulos, L. and Davies, R.: Plane parallel albedo biases from satellite observations, Part II: Parameterizations for bias removal, *J. Climate*, 11, 933–944, 1998.
- Oreopoulos, L. and Khairoutdinov, M.: Overlap properties of clouds generated by a cloud-resolving model, *J. Geophys. Res.* 108, 4479, doi:10.1029/2002JD003329, 2003.
- 5 Oreopoulos, L. and Norris, P. M.: An analysis of cloud overlap at a midlatitude atmospheric observation facility, *Atmos. Chem. Phys.*, 11, 5557–5567, doi:10.5194/acp-11-5557-2011, 2011.
- Pincus, R., Barker, H. W., and Morcrette, J. J.: A fast, flexible, approximate technique for computing radiative transfer in inhomogeneous cloud fields, *J. Geophys. Res.*, 108, 4376, doi:10.1029/2002JD003322, 2003.
- 10 Pincus, R., Hannay, C., Klein, S. A., Xu, K.-M., and Hemler, R.: Overlap assumptions for assumed probability distribution function cloud schemes in large-scale models, *J. Geophys. Res.*, 110, D15S09, doi:10.1029/2004jd005100, 2005.
- Press, W. H., Teukolsky, S. A., Vetterling, W. T., and Flannery, B. P.: *Numerical Recipes in Fortran 77, the Art of Scientific Computing*, 2nd Edn., Cambridge University Press, Cambridge, 933 pp., 1992.
- 15 Räisänen, P., Barker, H. W., Khairoutdinov, M., Li, J., and Randall, D. A.: Stochastic generation of subgrid-scale cloudy columns for large-scale models, *Q. J. R. Meteor. Soc.*, 130, 2047–2067, 2004.
- 20 Rienecker, M. M., Suarez, M. J., Todling, R., Bacmeister, J., Takacs, L., Liu, H.-C., Gu, W., Sienkiewicz, M., Koster, R. D., Gelaro, R., Stajner, I., and Nielsen, J. E.: The GEOS-5 Data Assimilation System – Documentation of Versions 5.0.1, 5.1.0, and 5.2.0, NASA/TM-2008-104606, 27, 118 pp., 2008.
- Shonk, J. K. P. and Hogan R. J.: Effect of improving representation of horizontal and vertical cloud structure on the earth's global radiation budget. Part II: the global effects, *Q. J. R. Meteor. Soc.*, 136, 1205–1215, doi:10.1002/qj.646, 2010.
- 25 Stephens, G. L., Vane, D., Boain, R., Mace, G., Sassen, K., Wang, Z., Illingworth, A., O'Connor, E., Rossow, W., Durden, S., Miller, S., Austin, R., Benedetti, A., Mitrescu, C., and Cloud-Sat Science Team: A new dimension of space-based observations of clouds and precipitation, *B. Am. Meteorol. Soc.*, 83, 1771–1790, 2002.
- 30 Sud, Y. C. and Lee, D.: Parameterization of aerosol indirect effect to complement McRAS cloud scheme and its evaluation with the 3-year ARM-SGP analyzed data for single column models, *Atmos. Res.*, 86, 105–125, 2007.

- Tian, L. and Curry, J. A.: Cloud overlap statistics, *J. Geophys. Res.*, 94, 9925–9935, 1989.
- Wilks, D. S.: *Statistical Methods in the Atmospheric Sciences*, Academic Press, New York, 464 pp., 1995.
- 5 Winker, D. M., Pelon, J., Coakley, J. A., Ackerman, S. A., Charlson, R., Colarco, P. R., Flamant, P., Fu, Q., Hoff, R. M., Kittaka, C., Kubar, T. L., Le Treut, H., MvCormick, M. P., Megie, G., Poole, L., Powell, K., Trepte, C., Vaughan, M. A., and Wielicki, B. A.: The CALIPSO mission: a global 3-D view of aerosols and clouds, *B. Am. Meteorol. Soc.*, 91, 1211–1229, 2010.

Radiative impacts of cloud heterogeneity and overlap in an atmospheric GCM

L. Oreopoulos et al.

[Title Page](#)[Abstract](#)[Introduction](#)[Conclusions](#)[References](#)[Tables](#)[Figures](#)[Back](#)[Close](#)[Full Screen / Esc](#)[Printer-friendly Version](#)[Interactive Discussion](#)

Radiative impacts of cloud heterogeneity and overlap in an atmospheric GCM

L. Oreopoulos et al.

Title Page

Abstract

Introduction

Conclusions

References

Tables

Figures

⏪

⏩

◀

▶

Back

Close

Full Screen / Esc

Printer-friendly Version

Interactive Discussion



Table 1. Parameters for the Gaussian fits per Eqs. (10) and (11) of zonal decorrelation lengths shown in Fig. 1.

Fit parameters for Eqs. (10) and (11)	Cloud fraction overlap	Condensate overlap
m_1	1.43	0.72
m_2	2.12	0.79
$m_{3,0}$	-7.00	-8.50
m_4	-25.58	40.40

Radiative impacts of cloud heterogeneity and overlap in an atmospheric GCM

L. Oreopoulos et al.

Table 2. List of experiments conducted with the GEOS-5 AGCM running two different cloud schemes to assess the effects of cloud hereogeneity and overlap on the cloud radiative effect.

Experiment ID	Description
1	Homogeneous clouds, maximum-random overlap
2	Heterogeneous clouds, maximum-random overlap, $L_r = 1$ km
3	Homogeneous clouds, generalized overlap, $L_\alpha = 2$ km
4	Heterogeneous clouds, generalized overlap, $L_\alpha = 2$ km, $L_r = 1$ km
5	As Exp. 4, but with weaker cloud heterogeneity
6	As Exp. 4, but with $L_\alpha = 4$ km, $L_r = 2$ km
7	As Exp. 4, but with $L_\alpha = 2$ km, $L_r = 2$ km
8	Heterogeneous clouds, generalized overlap from CloudSat/CALIPSO

Title Page

Abstract

Introduction

Conclusions

References

Tables

Figures

⏪

⏩

◀

▶

Back

Close

Full Screen / Esc

Printer-friendly Version

Interactive Discussion



Radiative impacts of cloud heterogeneity and overlap in an atmospheric GCM

L. Oreopoulos et al.

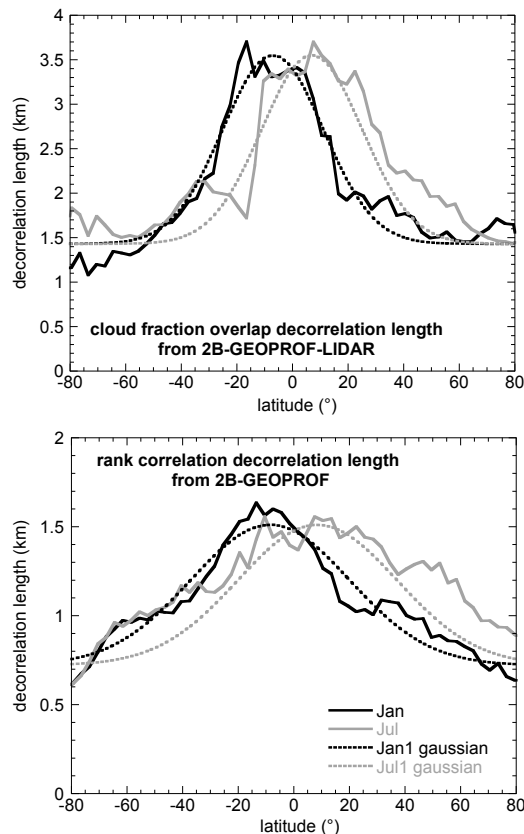


Fig. 1. (Top): cloud fraction overlap decorrelation lengths from 3° degree zonal averages of $\alpha(\Delta z)$ for January and July 2009 (solid curves) derived from the 2B-GEOPROF-LIDAR CloudSat product; the dashed curves are gaussian fits according to Eqs. (10) and (11). (Bottom): as top panel, but for rank correlation decorrelation lengths calculated from CloudSat 2B-GEOPROF CPR reflectivities.

Title Page

Abstract

Introduction

Conclusions

References

Tables

Figures

◀

▶

◀

▶

Back

Close

Full Screen / Esc

Printer-friendly Version

Interactive Discussion

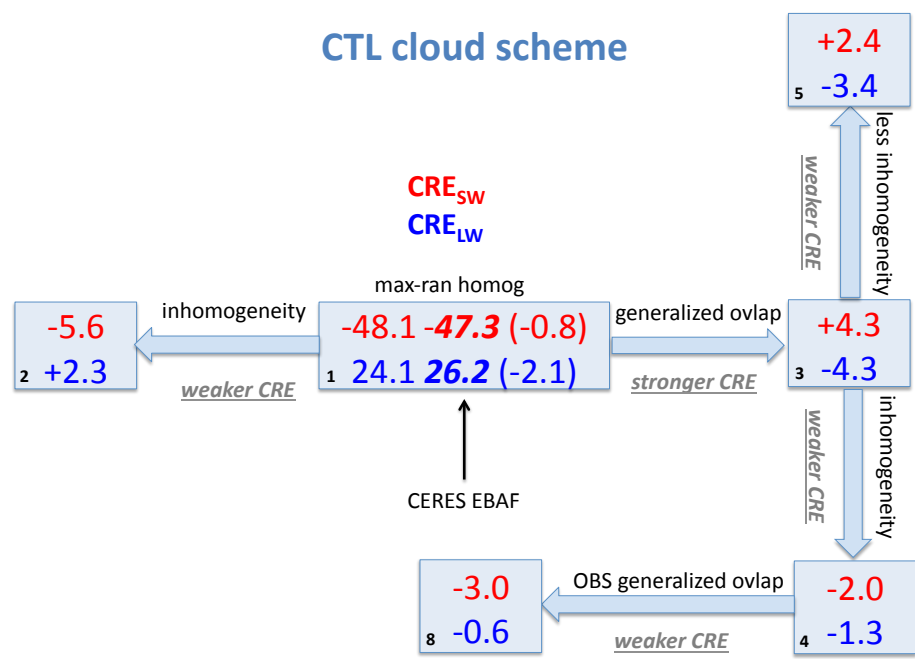


Fig. 2. Box chart providing diagnostic CRE changes (in $W m^{-2}$) when clouds condensate distributions are changed from homogeneous to heterogeneous and overlap changes from maximum-random to generalized for the cloud fields generated by the control (CTL) cloud scheme of GEOS-5. The changes are with respect to the reference values of diagnostic CRE (in $W m^{-2}$) in the center box (blue for CRE_{LW} , red for CRE_{SW}) produced assuming homogeneous clouds and maximum-random overlap (Exp. 1 in Table 2) within the RRTMG radiation package. Due to our sign convention, negative CRE_{LW} and positive CRE_{SW} changes from our reference values indicate stronger CRE. The numbers in italics in the center box are observed values from the CERES EBAF data set and the values in parentheses are differences between model reference CREs and CERES observed CREs. The numbers in the left bottom corner of the boxes are the experiment IDs according to Table 2.

Title Page

Abstract Introduction

Conclusions References

Tables Figures

⏪ ⏩

◀ ▶

Back Close

Full Screen / Esc

Printer-friendly Version

Interactive Discussion



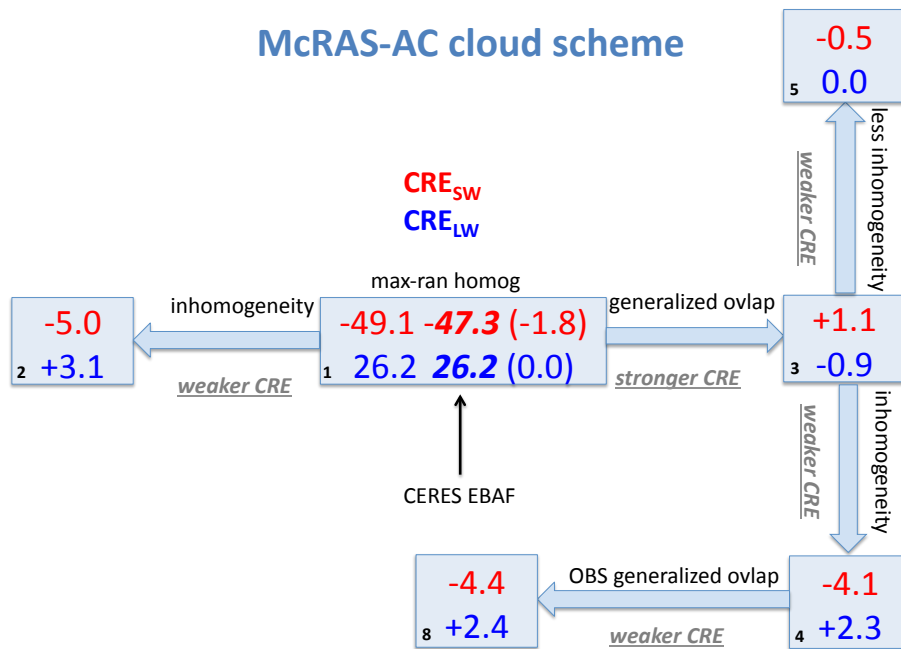


Fig. 3. As Fig. 3, but when McRAS-AC has replaced the GEOS-5 control cloud scheme.

[Title Page](#)
[Abstract](#)
[Introduction](#)
[Conclusions](#)
[References](#)
[Tables](#)
[Figures](#)
[◀](#)
[▶](#)
[◀](#)
[▶](#)
[Back](#)
[Close](#)
[Full Screen / Esc](#)
[Printer-friendly Version](#)
[Interactive Discussion](#)

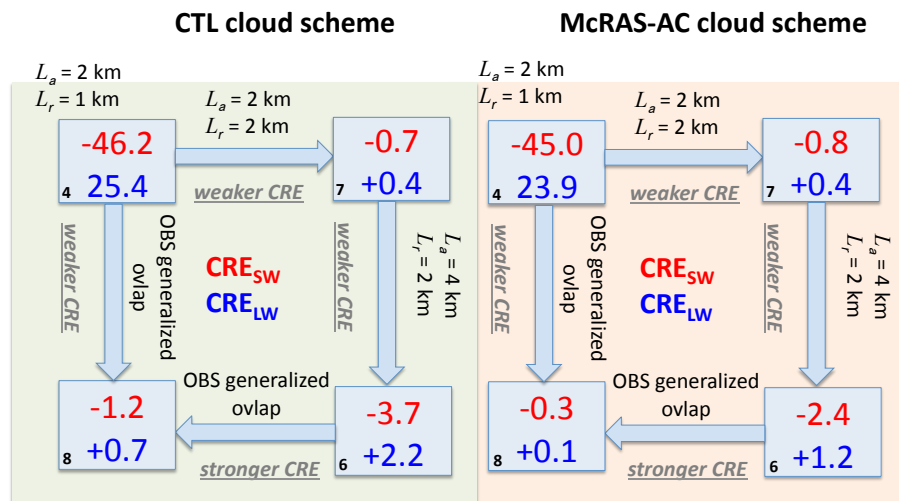


Fig. 4. CRE changes brought by changing the parameters (i.e., decorrelation lengths) of generalized overlap in the CTL cloud scheme (left) and the McRAS-AC cloud scheme (right). The reference CREs of the upper left box are from the simulation with heterogeneous clouds and generalized overlap with $L_a = 2$ km and $L_r = 1$ km (Exp. 4 in Table 2). The values shown in the other boxes are differences from the reference CREs for different experiments indicated by their IDs in the left bottom corner of the box according to Table 2.

Radiative impacts of cloud heterogeneity and overlap in an atmospheric GCM

L. Oreopoulos et al.

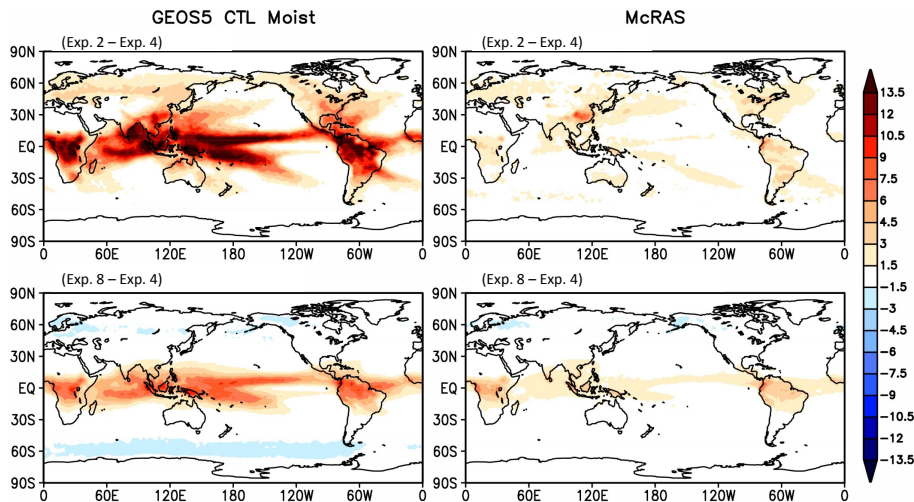


Fig. 5. Maps of annually averaged CRE_{SW} differences between the Exp. 2 and Exp. 4 (top) and between Exp. 8 and Exp. 4 (bottom). The left panels are for the CTL cloud scheme, while the right panels are for McRAS-AC.

Title Page

Abstract

Introduction

Conclusions

References

Tables

Figures

◀

▶

◀

▶

Back

Close

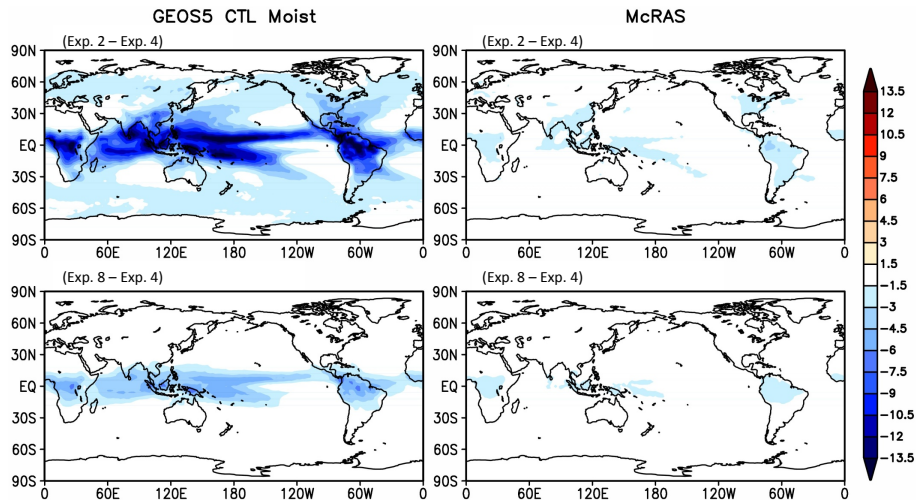
Full Screen / Esc

Printer-friendly Version

Interactive Discussion

**Radiative impacts of
cloud heterogeneity
and overlap in an
atmospheric GCM**

L. Oreopoulos et al.

**Fig. 6.** As Fig. 5, but for CRE_{LW}.[Title Page](#)[Abstract](#)[Introduction](#)[Conclusions](#)[References](#)[Tables](#)[Figures](#)[⏪](#)[⏩](#)[◀](#)[▶](#)[Back](#)[Close](#)[Full Screen / Esc](#)[Printer-friendly Version](#)[Interactive Discussion](#)

Radiative impacts of cloud heterogeneity and overlap in an atmospheric GCM

L. Oreopoulos et al.

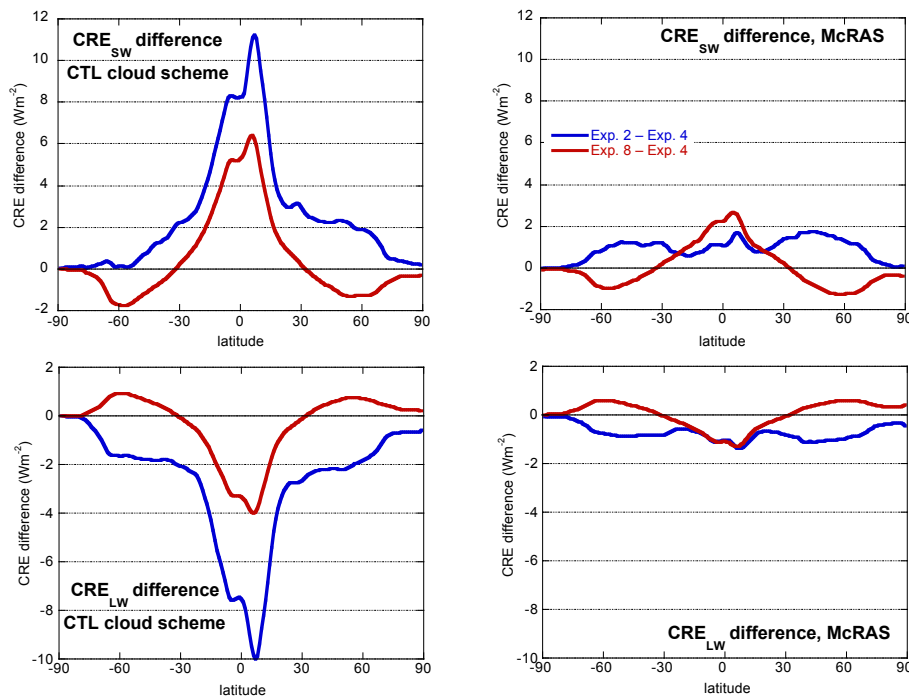


Fig. 7. Zonal averages of the differences shown in Figs. 5 and 6. The left panels are for the CTL cloud scheme, the right panels are for McRAS-AC. Top panels are for CRE_{SW} , while the bottom panels are for CRE_{LW} .

[Title Page](#)
[Abstract](#)
[Introduction](#)
[Conclusions](#)
[References](#)
[Tables](#)
[Figures](#)
[⏪](#)
[⏩](#)
[◀](#)
[▶](#)
[Back](#)
[Close](#)
[Full Screen / Esc](#)
[Printer-friendly Version](#)
[Interactive Discussion](#)

Radiative impacts of cloud heterogeneity and overlap in an atmospheric GCM

L. Oreopoulos et al.

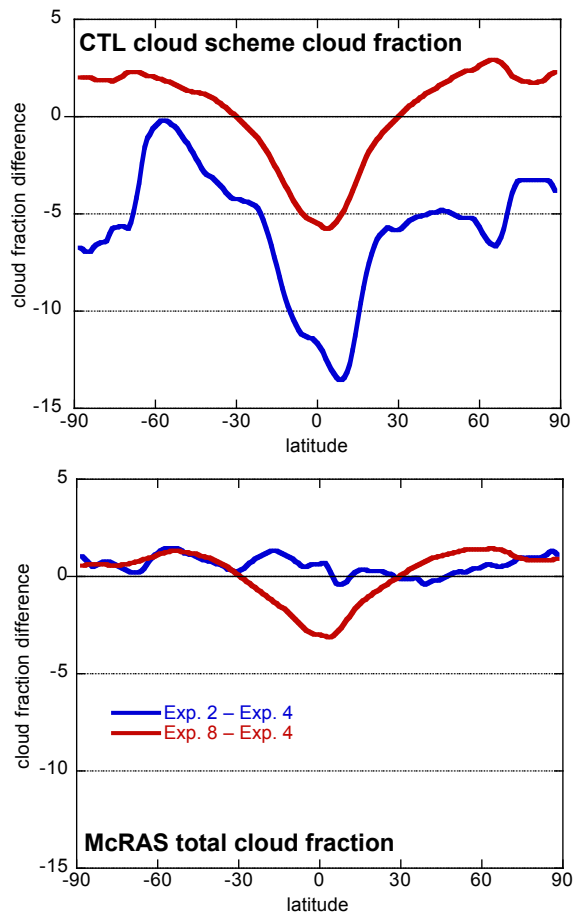


Fig. 8. Zonally-averaged differences of C_{tot} (on a scale 0–100) for Exp. 2–Exp. 4 (blue curves) and Exp. 8–Exp. 4 (red curves). The top panel is for the CTL cloud scheme, while the bottom panel is for McRAS-AC.

[Title Page](#)[Abstract](#)[Introduction](#)[Conclusions](#)[References](#)[Tables](#)[Figures](#)[◀](#)[▶](#)[◀](#)[▶](#)[Back](#)[Close](#)[Full Screen / Esc](#)[Printer-friendly Version](#)[Interactive Discussion](#)

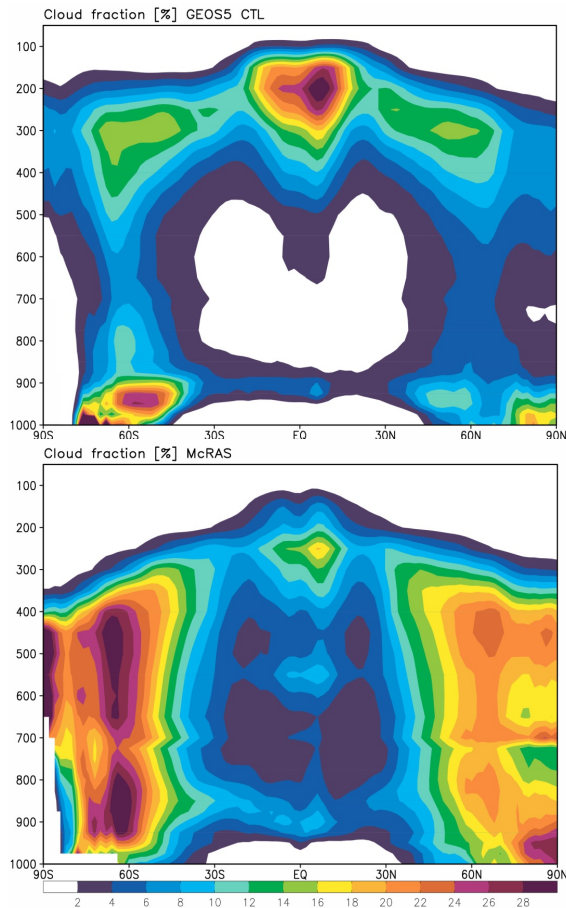


Fig. 9. Annually- and zonally-averaged cloud fraction profiles (on a scale 0–100) for the CTL and McRAS-AC cloud schemes.

Radiative impacts of cloud heterogeneity and overlap in an atmospheric GCM

L. Oreopoulos et al.

Title Page

Abstract Introduction

Conclusions References

Tables Figures

◀ ▶

◀ ▶

Back Close

Full Screen / Esc

Printer-friendly Version

Interactive Discussion



Radiative impacts of cloud heterogeneity and overlap in an atmospheric GCM

L. Oreopoulos et al.

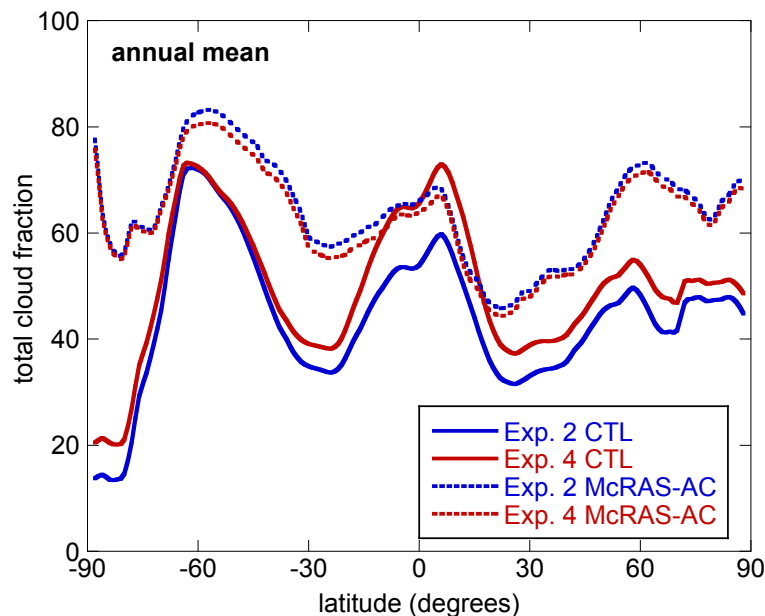


Fig. 10. Annually- and zonally-averaged total cloud fraction C_{tot} (on a scale 0–100) for Exp. 2 and Exp. 4 cloud fraction overlap assumptions applied to CTL and McRAS-AC cloud schemes.

[Title Page](#)[Abstract](#)[Introduction](#)[Conclusions](#)[References](#)[Tables](#)[Figures](#)[⏪](#)[⏩](#)[◀](#)[▶](#)[Back](#)[Close](#)[Full Screen / Esc](#)[Printer-friendly Version](#)[Interactive Discussion](#)

Radiative impacts of cloud heterogeneity and overlap in an atmospheric GCM

L. Oreopoulos et al.

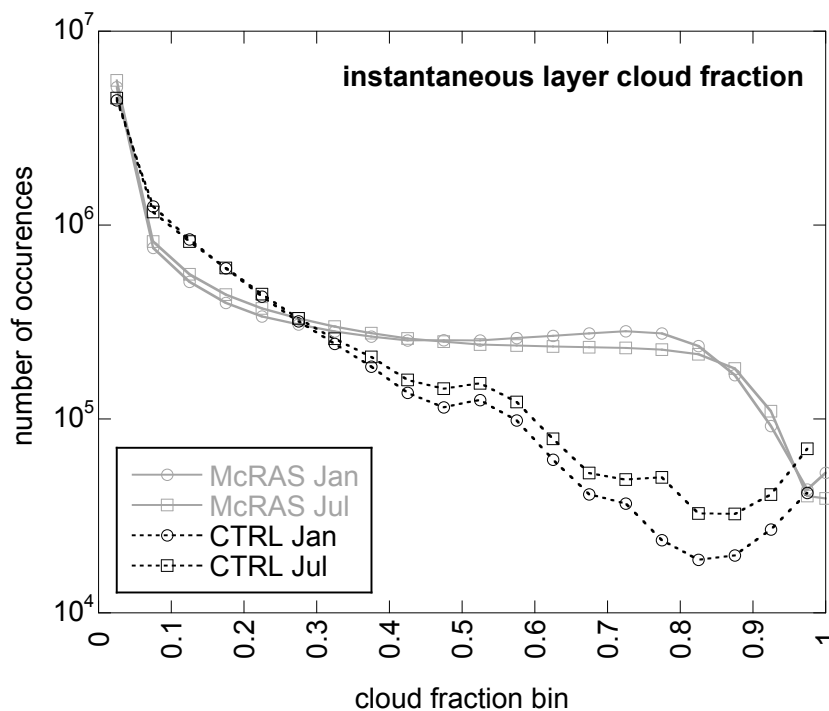


Fig. 11. Frequency distributions of twice-daily sampled instantaneous layer cloud fraction during January and July within the period of our runs. The cloud fraction bins are 0.05 wide, with a separate bin for completely overcast conditions.

[Title Page](#)[Abstract](#)[Introduction](#)[Conclusions](#)[References](#)[Tables](#)[Figures](#)[◀](#)[▶](#)[◀](#)[▶](#)[Back](#)[Close](#)[Full Screen / Esc](#)[Printer-friendly Version](#)[Interactive Discussion](#)

Radiative impacts of cloud heterogeneity and overlap in an atmospheric GCM

L. Oreopoulos et al.

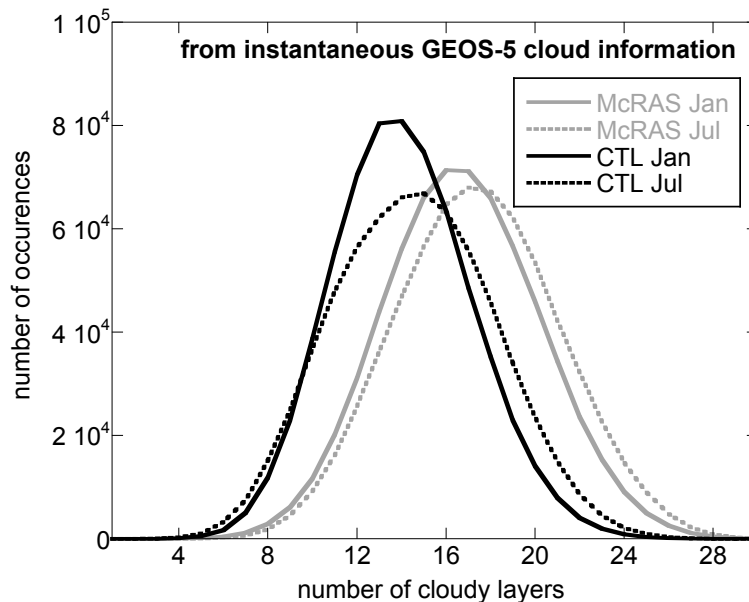


Fig. 12. Frequency distributions of instantaneous multi-layer cloud occurrences using the same data as in Fig. 11.

Title Page

Abstract Introduction

Conclusions References

Tables Figures

⏪ ⏩

◀ ▶

Back Close

Full Screen / Esc

Printer-friendly Version

Interactive Discussion

